Development of Harmonic Radar for Insect Detection

by

Fatima Mumtaz

Under the supervision of

Dr. Shobha Sundar Ram

Dr. Swapna Purandare

Indraprastha Institute of Information Technology Delhi

July 2019

Development of Harmonic Radar for Insect Detection

by

Fatima Mumtaz

Submitted
in partial fulfillment of requirements for the degree of
Master of Technology

to

Indraprastha Institute of Information Technology Delhi
July 2019

Certificate

This is to certify that the thesis titled "Development of Harmonic Radar for Insect Detection" being submitted by Fatima Mumtaz (Roll No.- MT17090) to the Indraprastha Institute of Information Technology Delhi, for the award of the Master of Technology, is an original work carried out by her under my supervision. In my opinion, thesis has reached the standards fulfilling the requirements of the regulations relating to the degree. The results contained in the thesis have not been submitted in part or full to any other university or institute for the award of any degree/diploma.

July, 2019

Dr. Shobha Sundar Ram
Assistant Professor
Department of Electronics and Communication Engineering
Indraprastha Institute of Information Technology, Delhi
New Delhi 110020

Dr. Swapna Purandare
Visiting Faculty (Ramanujan Fellow SERB-DST)
Department of Computational Biology
Indraprastha Institute of Information Technology, Delhi
New Delhi 110020

Abstract

Harmonic radar technology has been researched and developed for studying the foraging behaviour of insects such as honey bees in order to study their decline in the ecosystem. The traditional radar fails to detect the bees due to their very low radar cross-section caused by their small sizes. The harmonic radar overcomes this limitation by tagging the insects with a harmonic tag consisting of a dipole and a diode. The tag utilizes the non-linearity property of the diode to convert the carrier frequency of the transmitted signal received by the dipole to its harmonic components, which the dipole re-transmits to the radar. The radar detects the tag on the bee from the second harmonic in the received signal at the radar. This work presents the development of a working prototype of a first generation harmonic radar system to detect the presence of the insect tag at 2.5/5GHz. The thesis discusses the design methodology undertaken to build the radar using off-the-shelf components available in the institute lab. Based on empirical tests on the tag, we estimate the radar probability of detection and probability of false alarms as 88% and 0.3% respectively. The maximum detectable range for a monostatic configuration of the radar is 3.84 m.

Acknowledgements

I would like to express the deepest appreciation to my supervisors, Dr. Shobha Sundar Ram and Dr. Swapna Purandare, for their persistent support, guidance and patience. Without their valuable support, this thesis would not have been a success.

I would also like to thank Rahul Gupta, Khagendra Joshi, Abhijeet Mishra and Sana Ali Naqvi for extending their support with lab resources whenever needed. A special thanks to all my classmates and lab colleagues for the enjoyable discussions that helped in clarifying tough concepts and learning new ones.

This thesis is dedicated to my parents, my heroes, to whom I owe it all. To my brother for always being there and never giving up on me. And to my uncle, Dr. Majid Jamil, who counselled me to take up this incredible journey.

Contents

List of Figures

List of Tables

Chapter 1

Introduction

Insect pollinators play a vital role in the functioning of ecosystems. Their foraging behaviour dictates the out-crossing and reproduction of plants by transfer of pollen from male anther to female stigma of flowers [2]. Honey bees are recognized worldwide as one of the most important pollinating agents [3]. Thus the foraging pattern of honey bees is widely studied to understand their behaviour outside the hives which acts as a link to their in-colony activities. Forager bees are divided into scout (less in number) and reticent bees (larger in number). Outside the hives, scout bees are primarily involved in identifying best food resources and transferring the information to reticent bees in the colony. These identified resources are then visited by forager bees for nectar, water, pollen or resin collection [4]. Figure 1.1 shows a pictorial representation of forager bees leaving their hives to visit different flower beds to collect food. It is of interest to understand which resources are more preferred by a bee species over others, are they visiting the flower beds of same plant species or visiting flower beds of multiple plant species, how much time the bees spent on each flower bed, how far from the hive do they forage, does their foraging behaviour change with experience, do they keep exploring food resources over their lifetime or only in the initial days of their life amongst others. These questions can be answered by tracking bees over their entire lifespan [5]. The answers can help scientists understand the reason for the waning population of bees and agriculturists to strategize plant cultivation. Thus developing technology to help assist tracking the path of bees over their lifetime is crucial.

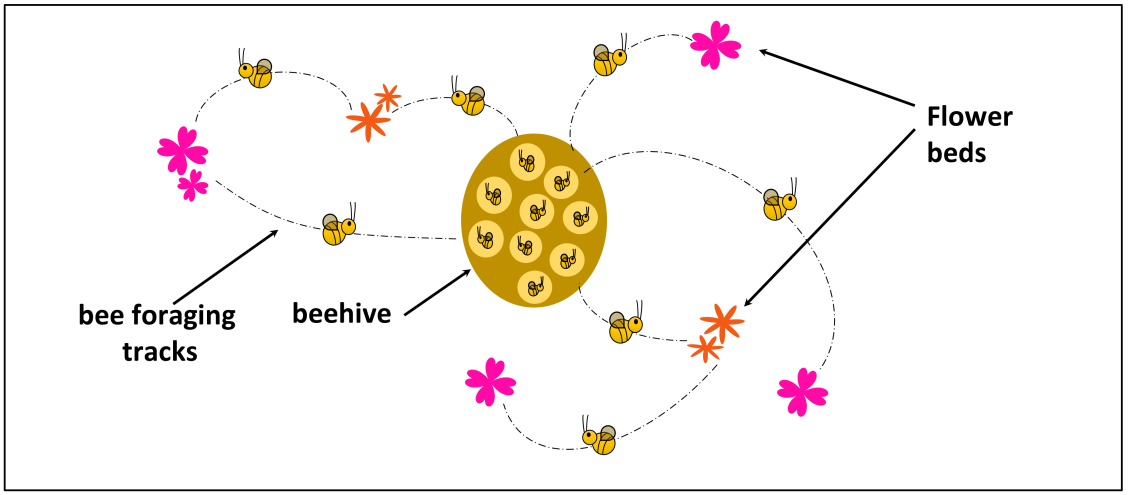

FIGURE 1.1: Pictorial representation of honey bees leaving their hives to collect food

1.1 Literature Survey

One of the technologies deployed for tracking insects is Radio Frequency Identification (RFID) technology. Many field studies have utilized the RFID technology to count the number of trips made by bees [6–10]. A passive RFID tag attached to the bee allows the RFID readers installed at the entrance of the hive to detect the bee whenever it enters or leaves the hive, allowing to keep count of the trips completed in a day. However, having very small working range, current RFID technology does not have the ability to perform localization of bees. Moreover, entrance and exit paths to the hives need to be defined for the bees, disturbing the natural habitat of the species.

Traditional radar has failed to track bees due to the low radar cross-section of the insect caused by its small size. As a result, the scattered signals from the radar are very weak and well below the noise floors of most radar receivers. Also, high ground clutter mask weak signals from targets. Harmonic radars are an alternative to the conventional radar and are used to detect and track cooperative targets. Here, a radar transmits a signal at a fundamental frequency. A passive harmonic tag is attached to a target insect, where harmonics of the received radar signal are generated. The radar receiver is tuned to receive one of the higher order harmonics, usually the second order harmonic. The received signal strength is thus a function of the electrical characteristics of the tag rather than the physical size of the insect. Hence, the tag can be designed so as to enable the detection of the insect even in the presence of noise and clutter. To ensure monitoring of bees over their lifetime, it is important to design a tag carefully so as to not cause

any hindrance to its movements and day to day activities. The tag must not rely on a perishable power source. The application of harmonic radar technology to track bees was first proposed in [1]. The radar consisted of a 9.4 GHz transmit frequency and 18.8 GHz receive frequency and 16 mm long lightweight tag comprising of a dipole, a diode and an inductive loop as detailed in [1, 11]. The harmonic radar has been successfully utilized in many field studies [5, 12–16]. It was observed that the tag does not seem to cause any abnormality in the foraging behaviour of the bee [17]. Many harmonic tag designs operating at different operating frequencies have been proposed. The tag designs explored different types of tag antennas including both wire and patch antennas [18, 19]. However, up to date the 16 mm dipole transponder is the most widely used tag design for field studies. Most of the field studies conducted upto date are done to track the Apis mellifera, a European honey bee species. We aim to study the foraging behaviour of Indian honey bees.

The harmonic radar system does not require any installation at the beehive entrance. This ensures that there is no interruption to the movement of bees in and out of the hive. An important advantage of harmonic radar over RFID technology is that it can provide co-ordinates for complete flight trajectories of bees over long ranges (hundreds of meters). Moreover, the performance. of radars is not affected by weather or presence of light unlike camera technology. However, a limitation of the harmonic radar is that it can only track one target at a time [5]. Thus multiple forager bees cannot be tracked simultaneously.

Based on the functionality and hardware complexity, the development of a harmonic radar system is structured across three generations as depicted in Fig. 1.2. The *first generation* harmonic radar aims to achieve detection of the target with the harmonic tag. The hardware configuration involves the use of a narrowband continuous wave radar with a single transmitter and receiver channel. The radar transmits at a fundamental frequency while the receiver is tuned for the second order harmonic. The *second generation radar* is envisaged as a broadband impulse radar that is modulated to the fundamental carrier frequency. The use of a wide bandwidth enables the range or distance estimation of the target. In other words, the radar would perform one-dimensional localization of the insect. The *third generation* radar would involve a broadband impulse radar with a multi-element receiver antenna array and corresponding receiver channels at the radar receiver. Through array processing, the direction-of-arrival of the insect

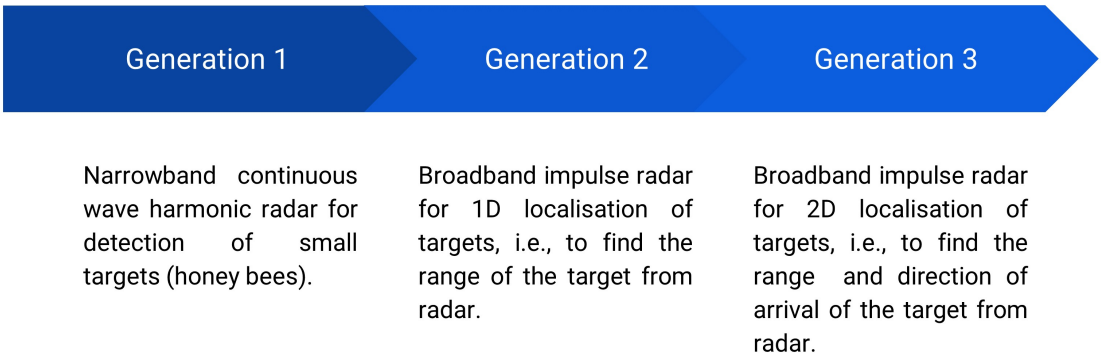

FIGURE 1.2: The three generations of harmonic radar system

along the azimuth would be determined thus enabling two-dimensional localization along both range and azimuth.

1.2 Thesis Objectives

The focus of my thesis is to develop the first generation harmonic radar for detecting Indian honey bees. The objectives of this thesis can be summarized as follows:

- To develop a working prototype for the first generation narrowband harmonic radar system using low cost off-the-shelf components available in the institute premises. This includes the continuous wave radar transmitter, receiver hardware and the design and development of the tag.
- To identify different radar configurations in terms of transmitter and receiver positions and evaluate the corresponding maximum detectable range of the radar target.
- To determine the performance constraints of the developed radar system in terms of probability of detection and probability of false alarms.
- To estimate the non-linearity coefficient of the tag and to test the tag for size and weight constraints on the Indian honey bee, Apis Dorsata.

1.3 Thesis Outline

This thesis is spread over five chapters. An overview of the upcoming chapters is briefed below:

- **Chapter 2: Introduction to Harmonic Radar**

  This chapter elaborates the principle of operation of a harmonic radar and draws a comparison between the traditional linear radar and the harmonic radar. Also, the non-linear radar range equation and non-linear radar cross section have been derived in this chapter. Finally, a performance comparison between linear and harmonic radar is drawn.

- **Chapter 3: Design Methodology**

  This chapter discusses in detail the various components of the transmitter, receiver and tag of the developed harmonic radar system.

- **Chapter 4: Results**

  This chapter presents the performance results of the developed harmonic radar system by finding the maximum detectable range, comparing mono-static and bi-static radar configurations for best performance and estimating the probability of detection and probability of false alarms of the developed system. The chapter also discusses the experiments conducted to estimate the non-linearity coefficient of the tag and test the tag for size and weight constraints on the Indian honey bee, Apis Dorsata.

- **Chapter 5: Conclusion**

  This chapter concludes the thesis by summarizing the outcomes of the thesis, stating the current hardware limitations and discussing the possible future work.

Chapter 2

Introduction to Harmonic Radar

This chapter discusses in detail the working of a harmonic radar and how it differs from the traditional radar. A narrowband radar system, illustrated in Fig. 2.1(a), comprises of a transmitter that generates and radiates an electromagnetic signal $s_I(t)$ of carrier frequency f_0 and strength a

$$s_I(t) = ae^{j2\pi f_0 t}. \tag{2.1}$$

The strength of the scattered radar signal by a non-cooperative target at the radar receiver is determined by target's radar cross-section (RCS), σ. The received signal at the radar, $s_R(t)$ is given by

$$s_R(t) = a\frac{\sqrt{\sigma}}{R^2}e^{j2\pi f_0(t-\frac{2R}{c})} \tag{2.2}$$

where R is the distance between the radar and the target and c is the speed of light. All the components of both the transmitter and receiver are tuned to the same fundamental frequency.

The block diagram of a harmonic radar is shown in Fig. 2.1(b). At the transmitter, the signal generator generates a continuous wave signal of carrier frequency f_0. A low pass filter is used to block any harmonics generated by the oscillator of the signal generator. The filtered signal is radiated in space by the transmitting antenna. In the case of a harmonic radar system, the target is a harmonic tag. The simplest configuration of a harmonic tag consists of an antenna (usually a dipole) and a diode. The antenna of the harmonic tag captures a portion of the signal transmitted by the radar giving rise to a

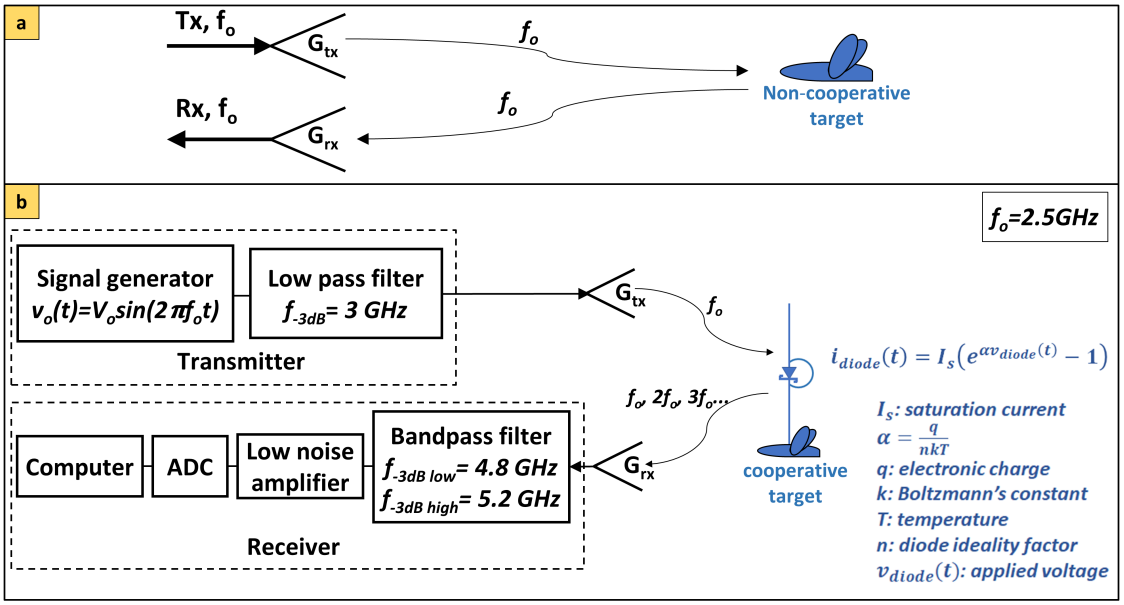

FIGURE 2.1: Block diagram representation of (a) traditional linear radar and (b) harmonic radar system

voltage, $v_{diode}(t)$, across the tag's diode

$$v_{diode}(t) = V_{diode} sin(2\pi f_0 t) \tag{2.3}$$

where V_{diode} is the amplitude of the signal. The diode current, i_{diode}, according to the Schockley diode equation is

$$i_{diode}(t) = I_s(e^{\alpha v_{diode}(t)} - 1) \tag{2.4}$$

where I_s is the reverse bias saturation current, $\alpha = \frac{q}{nkT}$, q is the electronic charge $(1.6 \times 10^{-19} C)$, n is the ideality factor of the diode, k is the Boltzmann constant and T is the absolute temperature ($290K$). Due to the non-linear nature of the current-voltage relationship of a diode, harmonics of f_0 are generated and re-radiated by the antenna. The radar receiver is tuned to receive the higher order harmonic - usually the second order. A band pass filter is used in the receiver to pass $2f_0$ while blocking f_0 that may be generated from the low noise amplifier (LNA) or tag. The digitized second harmonic signal from the ADC is then sent to the computer for further signal processing. The higher order harmonic at the radar receiver therefore indicates the presence of the target.

2.1 Non-linear Radar Range Equation

The radar range equation establishes a mathematical relation between the range of the radar and the characteristics of the transmitter, receiver, antennas, tag and environment [20]. In this section, the generalized radar range equation for non-linear systems has been derived [21].

Let $P_{tx}^{f_0}$ be the power transmitted by a radar located at the origin with a directional antenna of gain $G_{tx}^{f_0}(\theta, \phi)$ at frequency f_0. The power density impinging upon a harmonic tag placed at (R, θ, ϕ) from the radar is given by

$$S_{tx}^{f_0} = \frac{P_{tx}^{f_0} G_{tx}^{f_0}(\theta, \phi)}{4\pi R^2} \tag{2.5}$$

For λ_0 wavelength, the effective receive area $A_{tag}^{f_0}$ of the tag is

$$A_{tag}^{f_0} = \frac{\lambda_0^2 G_{tag}^{f_0}(\theta, \phi)}{4\pi}. \tag{2.6}$$

Then the amount of power absorbed by the tag's antenna, $P_{tag}^{f_0}$, is given by

$$P_{tag}^{f_0} = \frac{P_{tx}^{f_0} G_{tx}^{f_0}(\theta, \phi) A_{tag}^{f_0}}{4\pi R^2}. \tag{2.7}$$

A portion of the captured power passes through the non-linear diode where power harmonics are generated given by

$$P_{tag} = \sum_{n=1}^{\infty} P_{tag}^{nf_0} = \sum_{n=1}^{\infty} d_n (P_{tag}^{f_0})^n \tag{2.8}$$

where d_n is the scaling factor corresponding to the n^{th} harmonic with units $\frac{1}{W^{n-1}}$. The power density reflected back to the radar at distance R by the tag at n^{th} harmonic is proportional to the gain of the tag at nf_0

$$S_{rx}^{nf_0} = \frac{P_{tag}^{nf_0} G_{tag}^{nf_0}(\theta, \phi)}{4\pi R^2} \tag{2.9}$$

The received power at the radar is

$$P_{rx}^{nf_0} = S_{rx}^{nf_0} G_{rx}^{nf_0}(\theta, \phi) \frac{\lambda_0^2}{4\pi n^2} \tag{2.10}$$

where $G_{rx}^{nf_0}(\theta,\phi)$ is the gain of the radar receiving antenna at nf_0. Expanding the above equation we get the generalized form of the non-linear radar range equation,

$$P_{rx}^{nf_0} = \left[\left(P_{tx}^{f_0} G_{tx}^{f_0}(\theta,\phi)\right)^n G_{rx}^{nf_0}(\theta,\phi)\right]\left[G_{tag}^{nf_0} d_n (A_{tag}^{f_0})^n\right]\left[\frac{\lambda_0^2}{n^2(4\pi)^{n+2}R^{2n+2}}\right]. \quad (2.11)$$

The first set of terms in (2.11) are related to the radar system parameters such as the gain of the transmitting and receiving antennas and the transmitted power. The second set of terms correspond to the tag parameters while the third set of terms correspond to the free space loss.

2.2 Harmonic Radar Cross Section

Equation (2.11) reduces to the well known Frii's radar range equation when $n = 1$ corresponding to linear radars.

$$P_{rx}^{f_0} = \left[P_{tx}^{f_0} G_{tx}^{f_0}(\theta,\phi) G_{rx}^{f_0}(\theta,\phi)\right]\left[\sigma^{f_0}\right]\left[\frac{\lambda_0^2}{(4\pi)^3 R^4}\right] \quad (2.12)$$

where σ^{f_0} is the linear radar cross-section of the target that indicates the amount of signal returned by the target to the radar. Mathematically, σ^{f_0} is defined as [20]

$$\sigma^{f_0} = 4\pi \frac{P_{rx}^{f_0}}{S_{tx}^{f_0}}, \quad (2.13)$$

and is a function of the shape, material, physical area and aspect angle of the target and polarization and frequency of the transmitted signal. In the case of the harmonic radar, the RCS σ^{nf_0} is given by

$$\sigma^{nf_0} = 4\pi \frac{P_{rx}^{nf_0}}{S_{tx}^{f_0}} = d_n G_{tag}^{nf_0}(\theta,\phi)(A_{tag}^{f_0})^n. \quad (2.14)$$

Thus the harmonic radar cross-section is a function of the electrical properties of the tag such as the gain of the antenna and the non-linearity inherent in the diode. Therefore the harmonic radar is usually used only in situations where $\sigma^{nf_0} > \sigma^{f_0}$. This usually corresponds to situations where the target's linear radar cross-section is very low such as insects.

2.3 Performance comparison between linear radar and harmonic radar

The radar range equations in (2.11) and (2.12) reveal a number of key differences between the two types of radars:

1. For the same $P_{tx}^{f_0}, G_{tx}^{f_0}$, the higher order n results in increase in the received power for the harmonic radar.
2. However, for the same R, there is significantly greater free space loss in the system.
3. The strength of the non-linearity coefficients usually reduce with increase in n (i.e. $d_1 > d_2 > d_3 > \cdots$)
4. In the linear radar, both the transmitting and receiving antennas must operate at f_0, while for the harmonic radar, the receiving antenna must operate at nf_0.
5. In order for the tag to have high radar cross-section, it must have good gain at both f_0 and nf_0.

Based on the above considerations, we have explored the design of a second order harmonic radar with a dipole antenna in the tag.

Chapter 3

Design Methodology

This chapter discusses the design of the harmonic tag and the narrowband harmonic radar system consisting of the transmitter and receiver. We were guided by the philosophy of using cheap, off-the-shelf components and available laboratory resources. Our harmonic radar is designed to operate at 2.5GHz transmitting frequency and 5GHz receiving frequency. The choice of these frequencies is guided by the availability of hardware resources due to the popularity of these bands for WiFi and other wireless communication applications. In the following sections, we will describe the transmitter, receiver and the tag in greater detail.

3.1 Hardware description of the transmitter

Agilent N5181A MXG analog signal generator is used as the transmitter to generate a continuous wave sinusoidal signal at 2.5GHz. The signal generator can operate in the frequency range of 100kHz-3GHz and the maximum signal power supported by the device is 30dBm. The harmonic radar detection performance is susceptible to clutter from harmonics generated by the transmitting oscillator at high power. Therefore, we pass the generated signal through a customized microstrip low pass filter with a cut-off frequency at 3GHz. We implemented the filter on an FR4 substrate (relative permittivity = 4.7, thickness of dielectric = 1.5mm, copper thickness = 35um) [22]. We simulated the filter design in Advance Design System (ADS) software and fabricated it inside IIIT Delhi. The simulated and measured filter performances are shown in Fig. 3.1(a). We

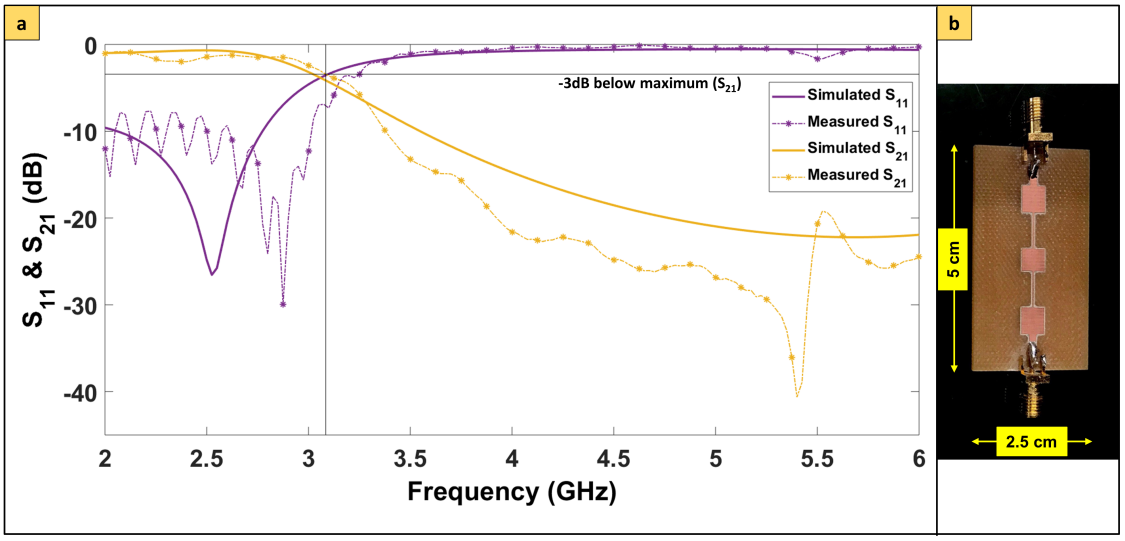

FIGURE 3.1: (a)Plot of the simulated and measured S_{11} and S_{21} parameters of the microstrip low pass filter with 3-dB cut-off of the fabricated filter at 3.085GHz highlighted by solid black lines. (b) Photograph of the microstrip low pass filter printed on FR4 board

observe the 3-dB cutoff frequency of the fabricated filter at 3.085GHz. The reflection scattering parameter, S_{11}, and the insertion scattering parameter, S_{21}, at 2.5GHz are -10.01dB and -1.74dB respectively. Figure 3.1(b) shows the photograph of the fabricated low pass filter.

The signal from the low pass filter is radiated via the transmitting antenna. The selection of the radar antennas was guided by empirical tests. The three antennas that were compared are a broadband R&S HF907 double rigid wave guide horn antenna of 8.91dBi gain at 2.5GHz, the Ettus VERT2450 dipole of 2dBi gain at 2.5GHz and a custom designed uniform linear array of 16 patch antenna elements shown in Fig.3.3. The elements of the array are fed by a corporate feeding network referenced from [23]. The patch array antenna, operational at 2.5 GHz, was fabricated on a FR4 substrate sheet (relative permittivity = 4.7, thickness of dielectric = 1.5mm, copper thickness = 35um). Simulations in CST Studio Suite software showed a peak gain of 11.6dBi at 2.5GHz as seen in the three-dimensional far-field directivity plot in Fig. 3.2(a). The simulated and measured S_{11} parameter is shown in Fig. 3.2(b). The photograph of the three antennas is shown in Fig. 3.3.

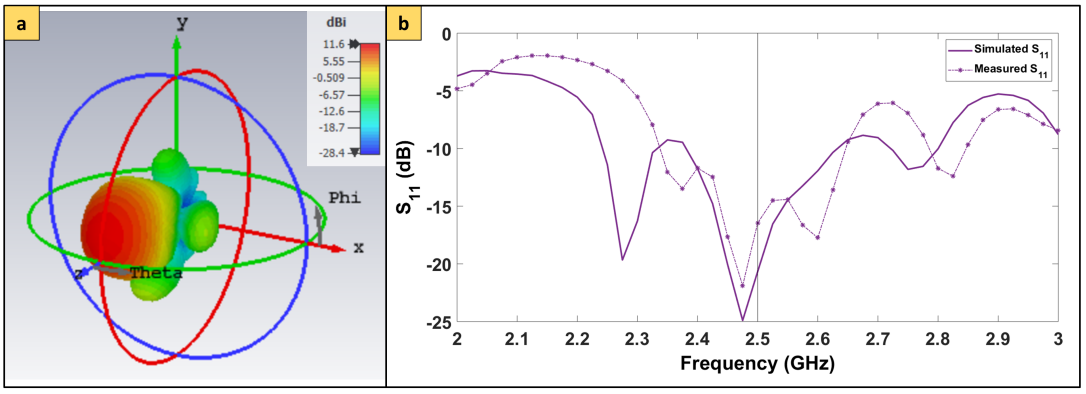

FIGURE 3.2: (a) Three-dimensional far-field directivity plot of the fabricated patch antenna and (b) Plot of simulated and measured s_{11} parameter

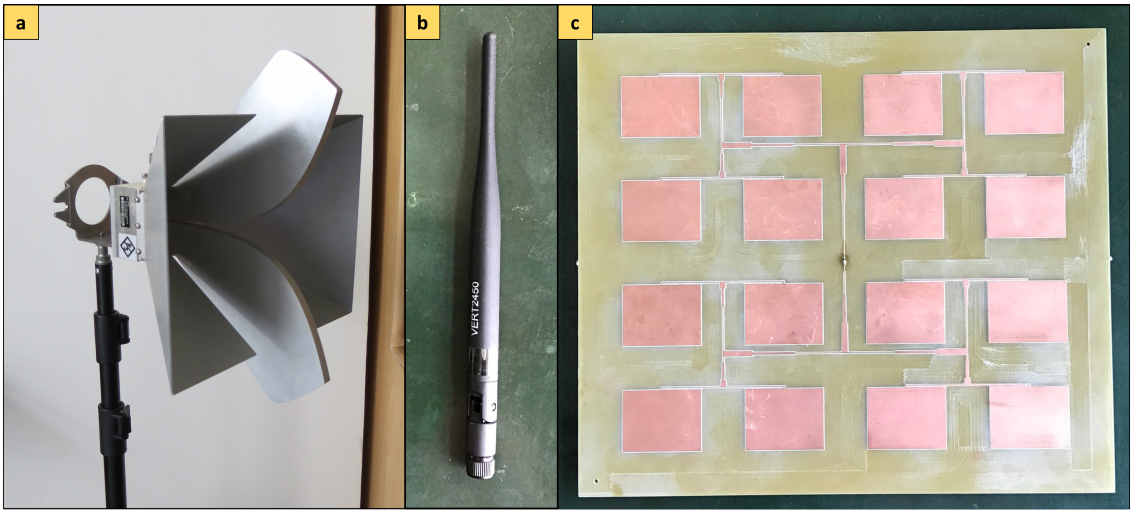

FIGURE 3.3: Photograph of (a) R&S HF907 Double rigid waveguide horn antenna (b) Ettus VERT2450 dipole antenna (c) Fabricated patch array antenna

3.2 Hardware description of the receiver

The signal from the tag is picked by the receiving antenna tuned to 5GHz. The possible choices for the receiver antenna are the horn (gain of 10.02dBi at 5GHz) and dipole antennas (gain of 2dBi at 5GHz) similar to those used in the transmitter. Before the received signal is further processed, it is imperative for the receiver to reject signals at 2.5GHz since they may give rise to higher order harmonics at the later amplification stages in the receiver chain. The two main sources of the fundamental frequency at the receiver are: (1) the direct signal from the transmitter (2) the reflected signal from the tag at the fundamental frequency. To overcome this issue, we use a custom designed microstrip coupled line band pass filter to block the fundamental frequency signals from entering the receiver chain while allowing second harmonic signal to pass through. The

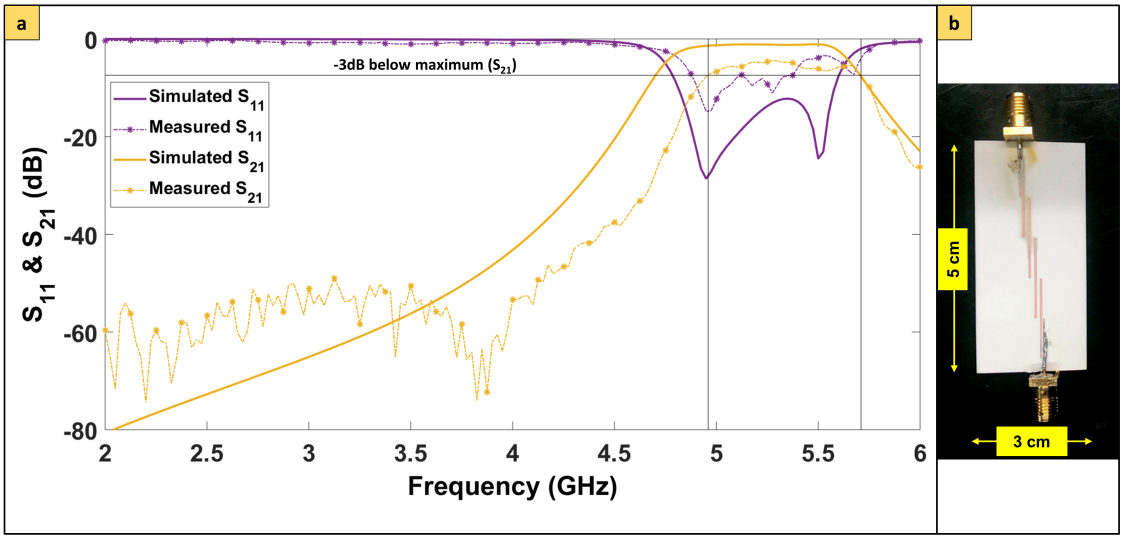

FIGURE 3.4: (a)Plot of the simulated and measured S_{11} and S_{21} parameters of the microstrip band pass filter. The lower 3-dB cut-off of the fabricated filter is at 4.96GHz and upper 3-dB cutoff is at 5.71GHz highlighted by solid black lines. (b) Photograph of the microstrip band pass filter printed on Rogers RO4003C board

filter is designed on a Rogers RO4003C (relative permittivity = 3.38, thickness of dielectric = 0.813mm, copper thickness = 35um) substrate [24]. The band filter is simulated in ADS software and fabricated in IIIT Delhi. Figure 3.4(a) shows the simulated as well as measured S_{11} and S_{21} parameters of the band pass filter. The measured lower cut-off frequency is 4.96GHz and the higher cut-off frequency is 5.71GHz. The measured S_{11} and S_{21} parameters at 5GHz are -12.32dB and -6.63dB respectively. The photograph of the fabricated band pass filter is shown in Fig. 3.4(b).

The filters were enclosed in an aluminum box to shield them from radio frequency interference and for making the design sturdy to handle the pressure from the RF cables and connectors. Please note that the band pass filter introduces a loss of -6.63dB. Hence, the use of the filter trades off between suppression of the fundamental frequency and the signal attenuation at 5GHz.

To measure the received signal, two receiver set-ups were experimented. In the initial set-up, the Agilent N9000A CXA signal analyser was used to perform analog to digital conversion and to display the signal in frequency domain. The noise floor of the signal analyser was -70dBm which is very high causing poor signal to noise ratio. A reduction in the noise floor is possible by lowering the resolution bandwidth and pre-amplifier gain. However, this results in very long data acquisition times which are not suitable for real time detection and tracking of targets. The size and weight of the device also posed

a limitation in terms of portability. Next, we considered the NI USRP-2921 Software Defined Radio module which is a tunable RF transceiver. The module comprises of an RF switch to transition between the transmitter and receiver chains. It streams baseband I and Q signals to host computer over a 1 Gigabit Ethernet. It is a half-duplex device. Hence it cannot be used for simultaneous transmission and reception. You also can use the USRP2921 for the following communications applications: implementing FM radio, direction finding, GPS simulation, development of passive radar, record and playback of RF signals amongst others. The device can receive signals in either the frequency range of 2.4-2.5GHz or 4.9-5.9GHz. Therefore, the receiver can be configured as a traditional radar or as a harmonic radar and their performances can be compared. The USRP offers considerable flexibility in the receiver parameters. The gain of the low noise amplifier was set at 10dB. We implemented receiver configuration with an intermediate frequency at 40 KHz in order to mitigate the effects of flicker noise in the circuitry. We selected a sampling frequency of 100KHz to save a time-domain signal of 10us duration. The received signal was time averaged to achieve a noise floor of -108 dBm. Due to the advantages of the USRP over the signal analyzer in terms of the noise performance, portability and speed of data acquisition, the USRP became the natural choice for the harmonic radar receiver. The USRP was connected via ethernet to the computer where the data were further processed.

3.3 Components of the Harmonic Tag

The harmonic tag consists of three components: a wire dipole antenna, a diode and an inductive loop.

The first component of the tag is the the wire dipole antenna that acts as a half-wave dipole at 2.5GHz and a full-wave dipole at 5GHz. The half-wave dipole at 2.5GHz receives the signal transmitted from the radar and the full-wave dipole at 5GHz transmits the second harmonic generated by the diode back to the radar. The advantage of using this antenna design is four-fold. Firstly, utilising the same antenna for transmission and reception saves up on the the size of the tag. Secondly, the vertically standing structure of a wire dipole is advantageous for small insect targets as it can be mounted on a very small area on the insect body causing minimal interference with the insects legs and wings. Thirdly, the dipole has an omni-directional radiation pattern which would

enable the detection of the insect along different orientations. Lastly, the dipole has a fat doughnut shaped directivity pattern making it less susceptible to large fluctuations in performance with small antenna tilts. The fabricated dipole is 60mm in length. The wire used is an un-insulated copper wire of 0.5mm thickness.

The dipole antenna transfers the received signal at f_0 to the diode attached to its feed point. The signal triggers the diode to produce the diode current that contains the incident frequency (f_0) and the harmonics of the incident signal frequency ($2f_0$,$3f_0$,$4f_0$...) because of its non-linear property. We considered four off-the-shelf diodes for our design - SMS7630-079LF, BAT15-03W, HSMS-286K-BLKG and SMV1249-079LF. All these four diodes are rated to work at the desired radar frequencies. The first three are Schottky diodes while the last one is a junction tuning varactor diode. We performed an experiment to test the frequency conversion operation of the four diodes. The laboratory set up is shown in Fig. 3.5. In our experiment, we fabricated four tags, each with a half-wave dipole and a diode connected at its feed point. The feed point is connected to an SMA connector through which the tag is connected directly to a signal generator that transmits 2.5GHz continuous wave signal. The tag performs frequency conversion of the input signal and radiates the generated harmonics. A VERT2450 dipole receiver antenna is spaced 3m apart from the tag and the received signal is measured with the USRP. The receiver is first tuned to receive at 2.5GHz, and then at 5GHz. For each case, the transmitted power is varied and the received power is noted. The results of the experiment are shown in Fig. 3.6. The results show that the that the power received at 2.5GHz for all the diodes is almost comparable. However the following observations are made for received power at 5GHz: As the transmitted power increases, the reverse voltage in the diode increases. Hence we see improved performance at higher power levels. The received power is below the noise floor (-108dBm) for transmit power as high as -5dBm for all diodes. All three Schottky diodes outperform the varactor diode with HSMS-286K-BLKG performing the best. The superior performance of Schottky diodes is attributed to its low junction capacitance and low barrier that enables the diode to work at very low voltage levels as well. Moreover, the low cost, light-weight and miniature size of these diodes makes them ideal for insect tagging applications. A varactor diode has variable junction capacitance that decreases as reverse voltage increases. Thus, the low performance of varactor diode at low power levels is due to high junction capacitance.

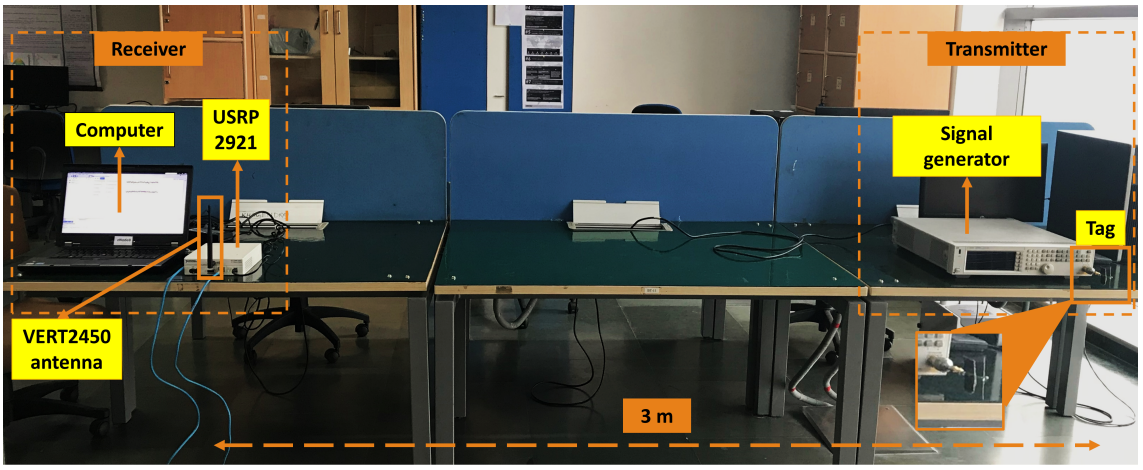

FIGURE 3.5: Experimental setup for one-way transmission with tag connected at transmitter end

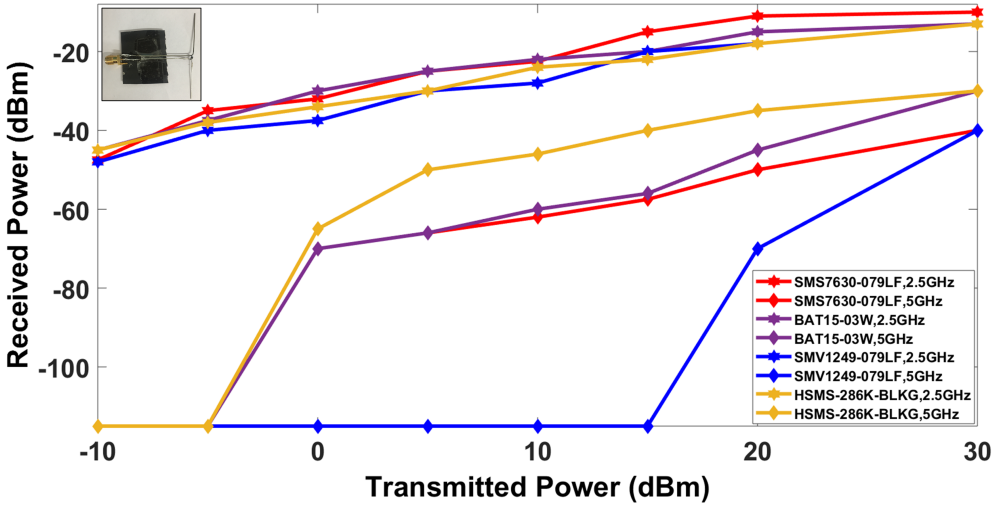

FIGURE 3.6: Plot of laboratory experiment to study the performance of diodes SMS7630-079LF, BAT15-03W, SMV1249-079LF and HSMS-286K-BLKG. The received power is plotted against the power transmitted from the signal generator (in dBm) at 2.5GHz and 5GHz.

In order to improve the efficiency of the tag, we incorporate an inductive loop across the diode. The inductive loop performs two major functions: (1) The loop acts as a direct current path allowing the flow of accumulated electrostatic charges thereby enabling the diode to operate in the zero-bias mode [19], (2) the loop helps in impedance matching the dipole with the diode to improve the efficiency of the overall tag performance. To understand how the loop helps in impedance matching, let us consider the Thevenin equivalent circuit of the tag at fundamental frequency f_0 as shown in Fig. 3.7(a). In the

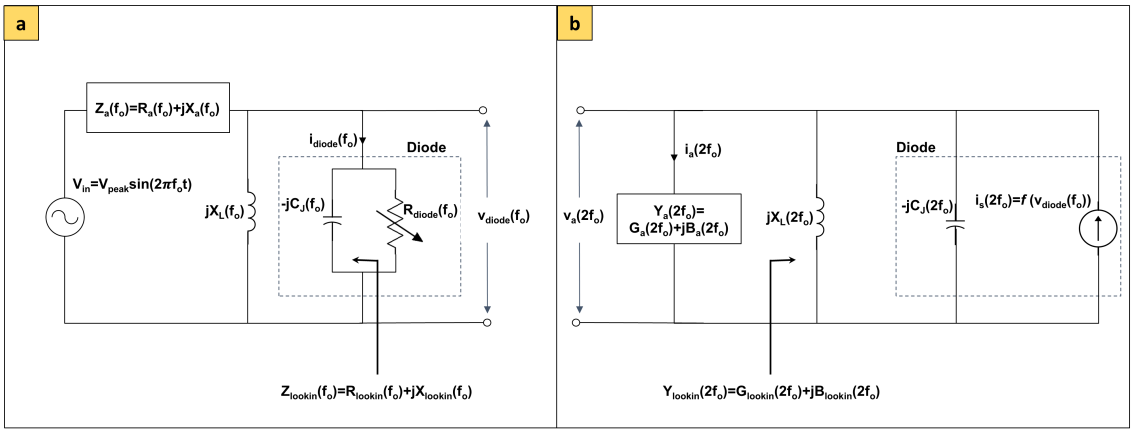

FIGURE 3.7: Circuit diagram representation of the harmonic tag at (a) 2.5 GHz (b) 5 GHz

circuit, $Z_a(f_0) = R_a(f_0) + jX_a(f_0)$ is the antenna impedance, C_j is the diode junction capacitance which is in parallel with the variable effective resistance of the diode R_{diode}.

The look-in impedance of the circuit is $Z_{lookin}(f_0) = R_{lookin}(f_0) + jX_{lookin}(f_0)$. At f_0, for maximum power transfer, $R_{lookin} = R_{diode}$ and $X_{lookin} = 0$ must hold true. For a half wave dipole, $R_a = 73\Omega$ and $X_a = 0$ due to resonance. However, R_{diode} attains very high values even for very low excitation levels. At second harmonic frequency, $2f_0$, the diode is modeled as a current source in parallel with the junction capacitance C_j. The Norton equivalent circuit at frequency $2f_0$ is shown in Fig. 3.7(b). The look-in admittance of the circuit is represented by $Y_{lookin}(2f_0) = G_{lookin}(2f_0) + jB_{lookin}(2f_0)$. Now the optimum performance of the tag and maximum power transfer can only be realized if impedance matching happens at both f_0 and $2f_0$. At f_0, $R_{diode} \neq R_a$. For maximum power transfer at $2f_0$, $G_a = G_{lookin}$ and $B_a = -B_{lookin}$ must hold true. For a full wave dipole at $2f_0$, $G_a \sim 0$ due to anti-resonance. Instead of choosing X_L value to be anti-resonant at f_0, we choose it to be anti-resonant at $2f_0$, thereby making $B_{lookin} = 0$ and $G_{lookin} = 0$. This will ensure maximum power transfer at $2f_0$. Since, this will make loop inductive at f_0, we design the dipole a little shorter than half-wavelength to make it capacitive at f_0.

A laboratory experiment was conducted to check the performance of the tag for different inductance values. Figure 3.8(e) shows a set of tags fabricated for different loop dimensions. Similar tags were fabricated for all four diodes mentioned above. The experiment uses the one-way transmission set-up shown in Fig. 3.5. The power transmitted by the signal generator was varied and the received power are presented in Fig. 3.8(a)-(d).

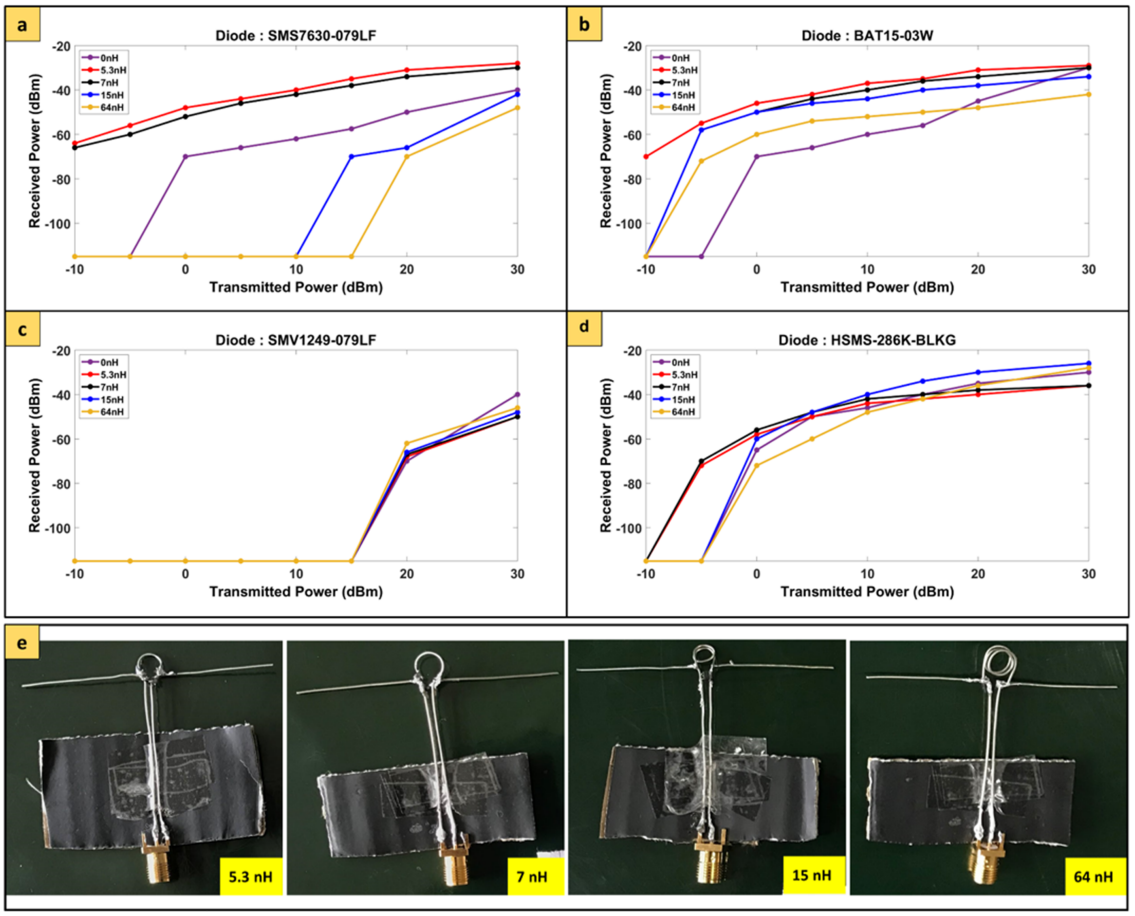

FIGURE 3.8: Plot of laboratory study of the performance of the tag by varying the value of inductance of the loop. The received power is plotted against the transmitted power from signal generator (in dBm) for diode (a) SMS7630-079LF, (b) BAT15-03W, (c) SMV1249-079LF and (d) HSMS-286K-BLKG respectively. (e) Photograph of a set of fabricated harmonic tags for SMS7630-079LF diode for different values of inductance of the loop. The inductance values of the loop for each tag is mentioned on the bottom left corner of each tag.

From the experiment, the following observations are made:

- Figure 3.8(a) shows the performance of SMS7630-079LF diode. It is seen that the tags with 5.3nH and 7nH loops have comparable performance. Increasing the loop inductance degrades the performance of the tag.
- Figure 3.8(b) shows the performance of BAT15-03W diode. It performs well for 5.3nH loop. The performance deteriorates for other inductance values.
- Figure 3.8(c) shows the performance of SMV1249-079LF diode. The tag is not detectable at transmitted power levels upto 15dBm with or without the loop.

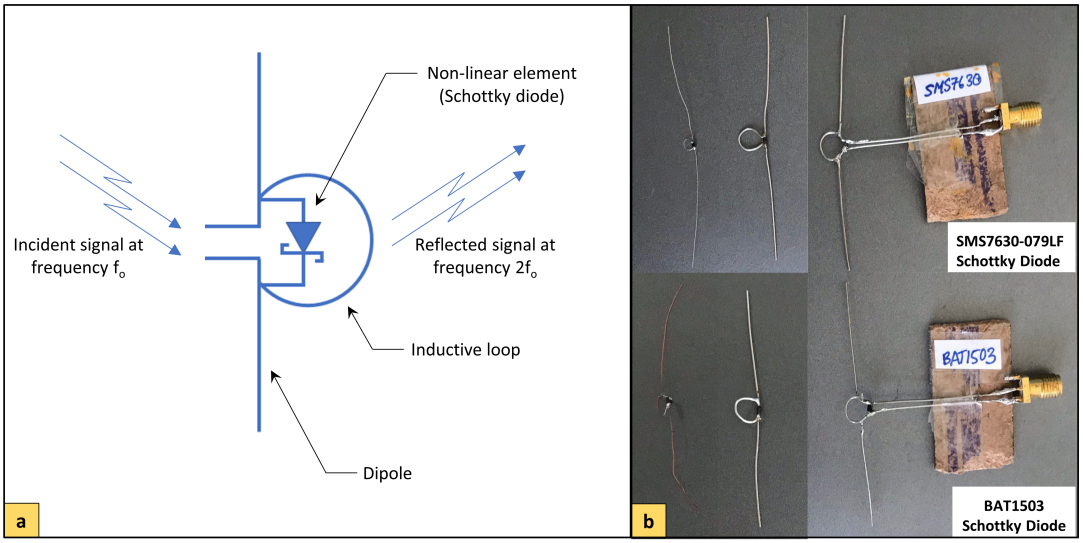

FIGURE 3.9: (a) Schematic diagram of harmonic tag (b) photograph of fabricated harmonic tags. The top row tags are fabricated with SMS7630-079LF diode and bottom row tags utilize BAT15-03W diode.

- Figure 3.8(d) shows the performance of HSMS-286K-BLKG diode. Though the tag performs well at high power levels, that received power is very low when the transmitted power level is below -10dBm.

Based on the above experiments, we shortlisted the SMS7630-079LF and BAT15-03W diodes and inductive loop of 5.3nH for fabrication of tag for further experiments. The schematic diagram of the complete tag is shown in Fig. 3.9(a) and Fig. 3.9(b) shows the picture of the fabricated tags.

Chapter 4

Results

In this section, we test the performance of the harmonic radar system and tag that were developed. We perform five experiments.

- The first experiment is to estimate the non-linearity coefficient of the tag.
- The second experiment is to determine the maximum detectable range of the tag.
- The third experiment is to compare monostatic and bistatic radar configurations in the laboratory set-up.
- The fourth experiment is to estimate the radar's probability of detection and false alarm as a function of the system's signal to noise ratio.
- The fifth experiment is to test the developed tag for size and weight constraints on the Indian honey bee, Apis Dorsata.

4.1 Estimation of non-linearity coefficient of harmonic tag

Figure 3.5 shows the experimental set-up used to find the non-linearity coefficient (d_2) of the harmonic tag. The tag is directly connected to the signal generator at the transmitting end. At the receiver, the VERT2450 dipole antenna is connected to the USRP. The distance between transmitter and receiver is 3m. The signal generator transmits a 2.5 GHz sinusoidal signal of 30 dBm power and the USRP is configured in the manner

discussed in Section 3.2. For this set-up, the power received at 5GHz was -28dBm. Using $P_{tx}^{f_0}$ and $P_{rx}^{2f_0}$ we find $d_2 = 0.2$ from

$$P_{rx}^{2f_0} = \frac{d_2 (P_{tag}^{f_0})^2 G_{tag}^{2f_0} G_{rx}^{2f_0} \lambda_0^2}{4(4\pi R)^2} \tag{4.1}$$

where $P_{tag}^{f_0} = P_{tx}^{f_0}$. The values of $G_{tag}^{2f_0} = 3.6\ dBi$ and $G_{rx}^{2f_0} = 2dBi$ were found from CST simulation of the dipole.

4.2 Estimation of maximum detectable range

The experimental set-up employed to find the maximum detectable range of the radar is shown in Fig. 4.1. In the set-up, we deploy a monostatic radar configuration, i.e., the transmitter and receiver are collocated. The transmitting chain comprises of the the signal generator, the low-pass filter and the horn antenna. At the receiver, the dipole antenna is connected to the USRP which is connected to the computer, via ethernet, where the amplitude of received power at 5GHz is displayed. The transmitter was configured to transmit 20dBm power and the USRP configuration for the experiment was kept the same as mentioned in Section 3.2. The tag was mounted on a stand that was moved away from the radar, along the radial direction, at intervals of 0.6m, until the received signal was below the noise floor (at -108dBm) and hence not detectable.

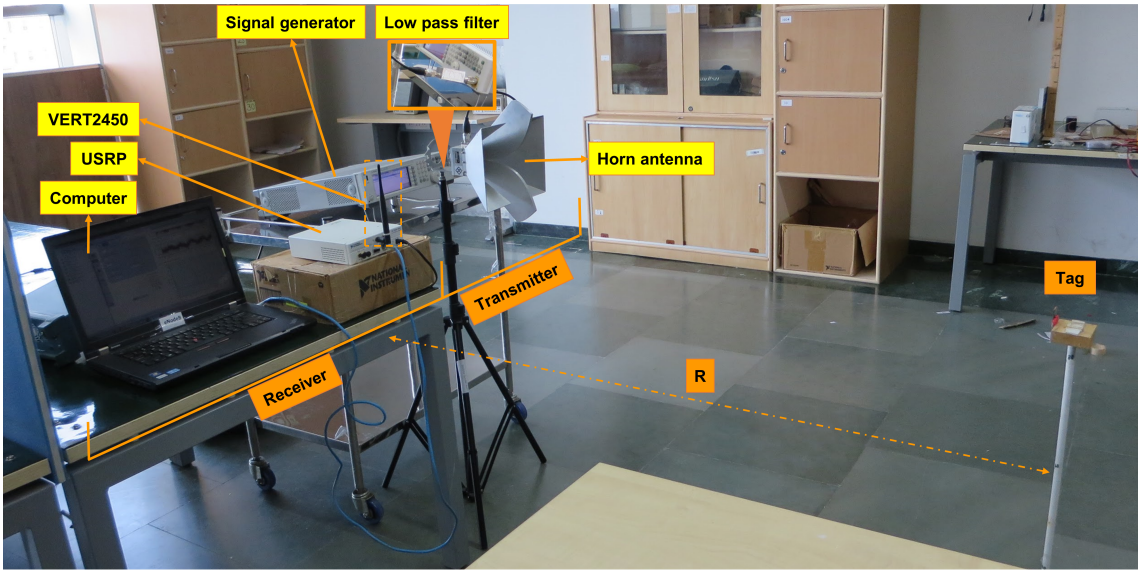

FIGURE 4.1: Experimental set-up for finding maximum detectable range of the radar

TABLE 4.1: The received power (in dBm) for different distances (in m) of the tag from the radar

Distance of tag from radar (m)	Received power (dBm)
0.6	-59
1.2	-79
1.8	-89
2.4	-97
3	-103
3.6	-105
3.84	-106
4.2	Below noise floor

Table 4.1 shows the received power from the tag for different distances of the tag from the radar. The maximum detectable range was recorded as 3.84m.

4.3 Comparison of monostatic and bistatic radar configurations

Since the path loss for two-way propagation is found to be high for monostatic configuration resulting in low coverage area for detection of targets, we conducted a study to check whether there is an improvement in the performance by implementing bistatic configuration.

For the study, we selected a controlled space that could eventually be used for laboratory experiments to monitor the activities of bees. We chose to use a double bed folding mosquito net shown in Fig. 4.2(a). The net is cheap, transparent, easy to assemble and disassemble and has the required dimensions for easy movement of bees.

We conducted five experiments to determine the radar configuration for obtaining the best coverage of the tag inside the net. The set up for the bistatic configuration with horn antennas at transmitter and receiver is shown in Fig. 4.3. For all the experiments, the transmitter comprised of the signal generator, low pass filter and transmitting antenna while the receiver comprised of the receiving antenna, USRP and computer.

In our experiments, we tested different types of radar antennas and antenna placement options. We considered the the horn, vertical dipole and the custom patch array for the transmitting antenna. The horn and vertical dipole were considered as possible choices for receiving antenna. We consider monostatic configuration where the transmitter and

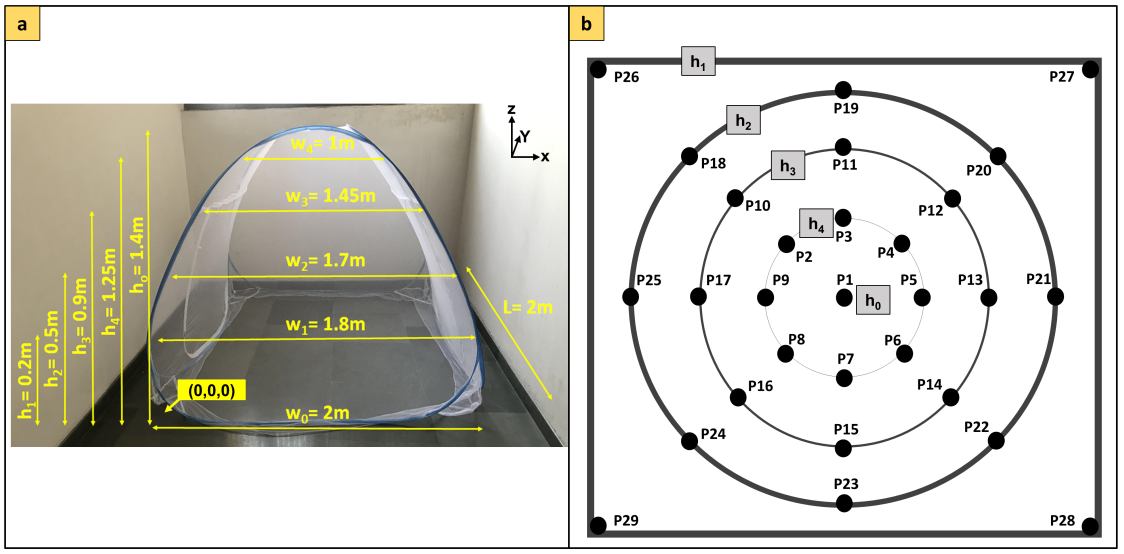

FIGURE 4.2: (a) Photograph of the mosquito net with dimensions (b) Top view of the net marked with contour lines depicting height of the points

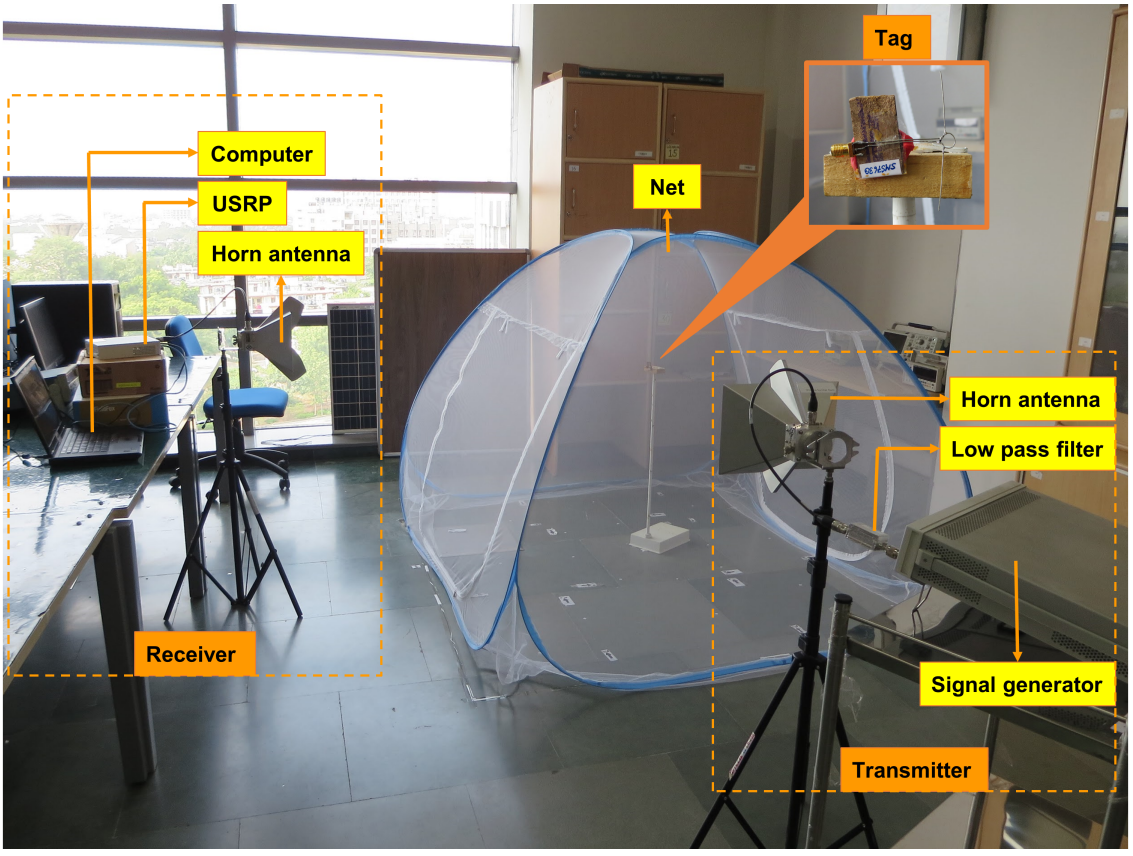

FIGURE 4.3: Experimental set-up for bistatic configuration with horn antenna as transmitting as well as receiving antenna

receiver are collocated as well as the bistatic configuration where the transmitter and receiver are separated. Figure 4.2(a) shows the origin [0,0,0] with respect to the net. The type and placement of transmitter and receiver antenna for each experiment is as follows:

- Experiment 1: The transmitter antenna is horn and receiving antenna is a vertical dipole placed at [2m, 0m, 1.1m] and [0.4m, 2m, 1.1m] respectively.
- Experiment 2: The transmitter and receiving antennas are vertical dipoles and placed at [2m, 0m, 1.1m] and [0.4m, 2m, 1.1m] respectively.
- Experiment 3: The transmitter antenna is the custom patch array while the receiving antenna is the vertical dipole. They are placed at the same positions as the previous cases.
- Experiment 4: The transmitter horn is placed at [2.9m, 1m, 1.1m] while the receiver horn is placed at [1m, -0.8m, 1.1m].
- Experiment 5: Both the transmitter and receiving antennas are vertical dipoles and collocated at [1m, 0.7m, 1.1m]. The transmitting antenna is mounted above the receiving antenna.

We measured the received power at the radar by placing the tag at 29 points at different positions and heights within the net. The recorded results are presented visually on the top view of the net. The dimensions of the net shown in Fig. 4.2(a) are matched to the placement of points in the top view of the net depicted in Fig. 4.2(b). The solid lines of varying thicknesses in the figure depict contour lines at different heights. For example, the outermost contour depicts a height of h_1=0.2m. Fig. 4.4(a)-(e) shows the amount of power received for experiments 1-4 respectively and Fig. 4.5 shows the received power for experiment 5. The color of the dots indicate the range of the strength of the received power (in dBm).

From the results it is observed that the bistatic radar configuration with horn antenna as transmitter as well as receiver gives maximum coverage of detection of tag (corresponding to Fig. 4.4(d)). This is because the horn antennas are characterized by the highest gains among the three antennas. Also, in a bistatic configuration, the strong direct coupling

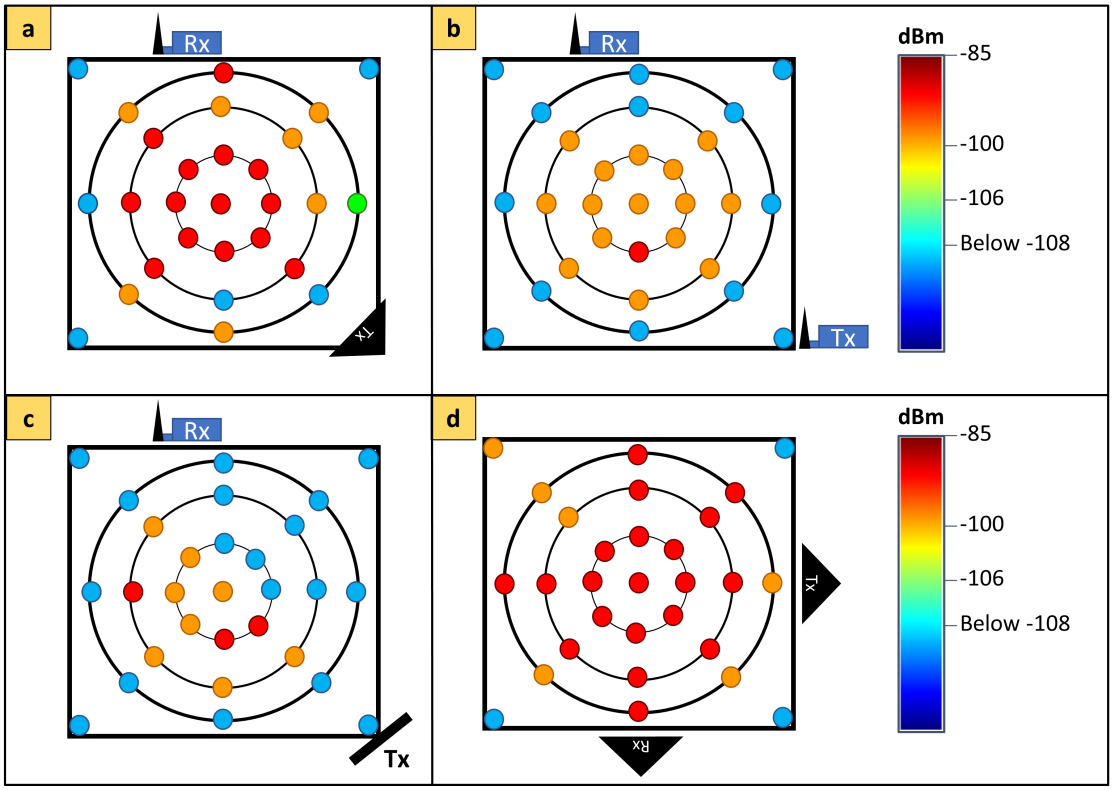

FIGURE 4.4: Plot of strength of power received with (a) horn as transmitter and dipole as receiver, (b) dipole as transmitter and dipole as receiver, (c) patch array as transmitter and dipole as receiver (d) horn as transmitter and horn as receiver for bi-static set-up

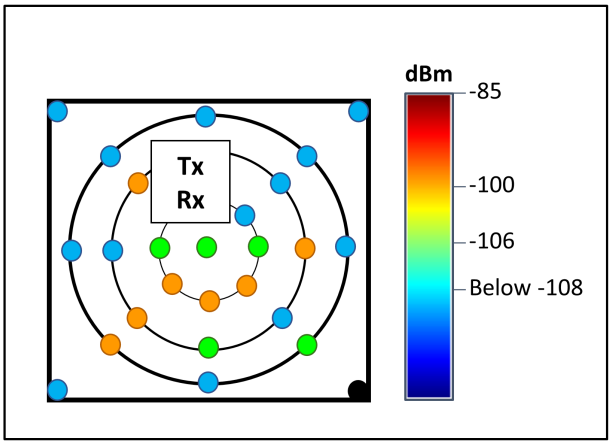

FIGURE 4.5: Plot of strength of power received with dipole as transmitter and dipole as receiver for mono-static set-up with the radar placed inside the net

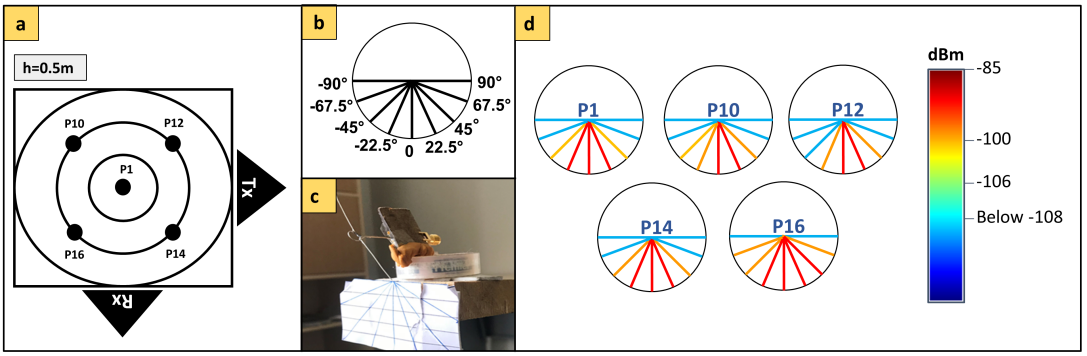

FIGURE 4.6: (a) Top view of the net showing position and height of the 5 points considered for the experiment to find the effect of tilt on the performance of the tag (b) Pictorial representation of the angles at which the measurements are taken (c) Photograph of the tag mounted on the stand with angle markings (d) Received power intensity plot with horn antenna at transmitter and receiver when tag is rotated at different angles at height=0.5m at 5 different locations (P1,P10,P12,P14 and P16) as indicated in (a)

between the transmitter and receiver is reduced. In the configuration, the entire radar system is placed outside the net.

A tilt in the tag can result in polarization mismatch loss. So, we next performed an experiment to estimate the effect of polarization mismatch loss on the detection performance of the radar. For this experiment, we used the bistatic configuration used in experiment 4. The experimental set-up is shown in Fig. 4.3. The tag was mounted on the stand at a height of 0.5m. The result was recorded by placing the tag at 5 different positions as shown in Fig. 4.6(a). At each position, we considered 9 different tilts 22.5° apart that are pictorially represented as shown in Fig. 4.6(b). Figure 4.6(c) shows the photograph of tag mounted on the stand with tilt markings for the experiment. The results of the experiment are presented in Fig. 4.6(d). The color of the lines represent the strength of received power. The result shows that the tag is detectable up to 45° tilt from the vertical (-3dB polarization mismatch loss) in most cases.

4.4 Detection performance

Next, we evaluated the probability of detection and false alarm for the system using Monte Carlo simulations. We modeled the transmitted power $P_{tx}^{f_0}$ as 30dBm for $f_0 = 2.5GHz$. We modeled the position coordinates of the tag as a random three dimensional vector that could lie anywhere within a cuboid of dimensions comparable to the net (

$2m \times 2m \times 1.4m$) with uniform probability. The transmitting and receiving antenna were modeled at positions $[2.9 \times 1m \times 1.1m]$ and $[1m \times -0.8m \times 1.1m]$. If $R_{tx \to tag}$ is the distance of the tag from the transmitter and $R_{tag \to rx}$ is the distance of the tag from the receiver, then the received power at $2f_0$ can be calculated from a modified monostatic harmonic radar range equation, presented in (2.11), as:

$$P_{rx}^{2f_0} = \left[\left(P_{tx}^{f_0} G_{tx}^{f_0}(\theta_i, \phi_i)\right)^2 G_{rx}^{2f_0}(\theta_r, \phi_r)\right] \left[\mathbf{G_{tag}^{2f_0}} d_2 (\mathbf{A_{tag}^{f_0}})^2\right] \left[\frac{\lambda_0^2}{4(4\pi)^4 R_{tx \to tag}^4 R_{tag \to rx}^2 L}\right]. \tag{4.2}$$

Gains of the transmitting and receiving antenna were chosen to correspond to those of the HF907 horn antenna at f_0 and $2f_0$. Note that the gains of the the radar and the tag antennas vary with the azimuth and elevation aspect of the tag with respect to the radar. The non-linear radar cross section was modelled as a random variable with a Gaussian distribution ($N(0, 2.46)$) to incorporate the variations due to the tilt of the tag. From Section 4.1, the value of d_2 was taken to be 0.2. Cable losses (L) of 3 dB was considered. Once the received power was simulated, we added white Gaussian noise of $N(0, 0.0914)$. The histogram of the received signal and noise was simulated in MATLAB for 12412 Monte Carlo trials and presented in Fig. 4.7(a). The receiver noise characteristics were estimated from the noise floor of the USRP at 5GHz by running the receiver hardware without switching on the transmitter. The noise histogram is also plotted in the figure. The probability of detection (P_d) is given by the area under the histogram of the received signal and noise power above a pre-defined threshold (γ). The probability of false alarm (P_{fa}) is the area under the histogram of the noise power above the same threshold. The P_{fa} and P_d are plotted as a function of γ in Fig. 4.7(b). Based on the figure, the value of γ is selected as -107.5dBm to reduce the probability of false alarm to 0.29% while maximizing probability of detection to 88.25%.

4.5 Tagging the bee

An experiment was conducted to tag a wild species of bee found in India, the Apis Dorsata [25]. It is the largest Indian honey bee, 17-20mm in length and weighs 159.9 ± 15.5mg. We studied methods to mount the tag on the thorax of bee in a vertically upright position. The location and orientation was chosen strategically to cause no hindrance to the flight of the bee [11].

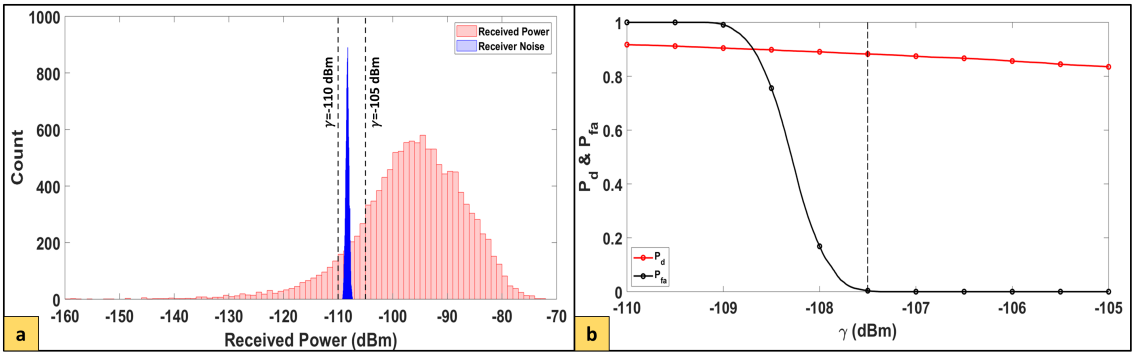

FIGURE 4.7: (a) Histogram plot of the receiver power and noise level of the radar system (b) Plot of probability of detection (P_d) and probability of false alarm (P_{fa}) as a function of threshold (γ) varying from -110dBm to -105dBm

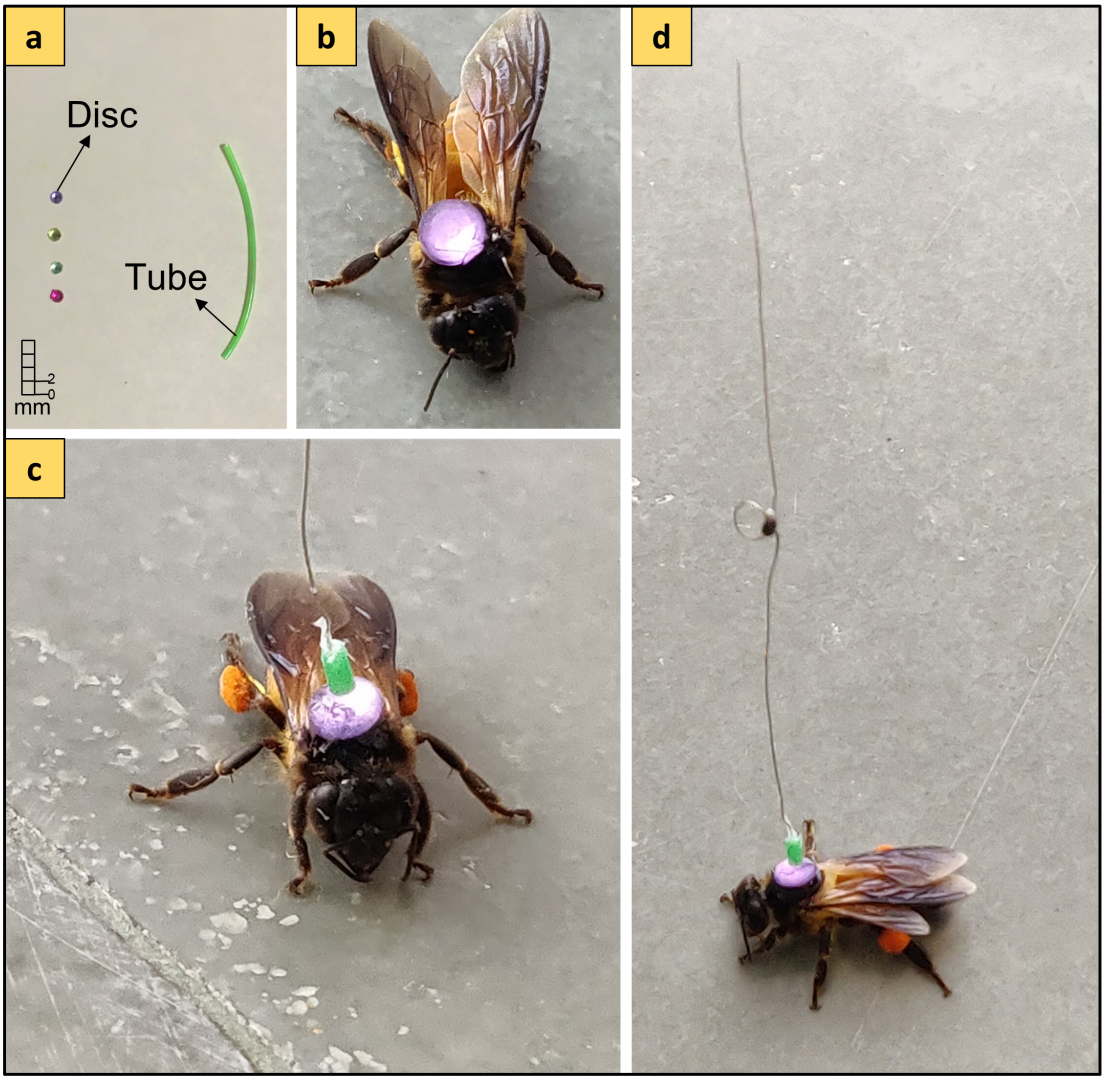

FIGURE 4.8: (a) Photograph of the disc and the tube that is used to create support for mounting the tag on the bee, (b) disc attached to the bee, (c) close up of the bee with the fitted tag, (d) photograph of the bee with the tag

The tag could not be directly attached on to the bee because of the small cross-sectional area of the wire dipole. Also, there is a possibility that the radiation from the bees body will affect the performance of the tag. Opalith discs are miniature round discs widely used by beekeepers to mark bees for studies by gluing it to the thorax [26]. These discs provide a good base to attach the tag. Due to unavailability of Opalith discs in Indian market, small craft rhinestone gems (shown in Figure 4.8(a)) that are readily available in craft shops were used as an alternative. Figure 4.8(b) shows the picture of a bee with the disc attached to its thorax. The tag (with dipole wire thickness of 0.5mm) was fixed to the disc. The disc was then glued to the bee. The bee was immobilized by refrigeration method discussed in [26]. It was observed that the bee was not able to maintain its balance and stand straight. Thus it was confirmed that the tag was too heavy for the bee. So another tag with 0.1mm uninsulated copper wire was fabricated. The tag was too thin to be directly attached to the disc. To support the tag, a flexible plastic tube (shown in Figure 4.8(a)) was attached to the disc. The tag was fixated in the tube using glue. This tag was then attached to the bee. With this tag on, it was observed that the bee was able to maintain its balance while walking. Figure 4.8(c) and (d) show the bee with the complete tag.

Chapter 5

Conclusion

In this thesis, a working prototype of the first generation narrowband harmonic radar, comprising of a transmitter, receiver and harmonic tag, have been successfully developed using off-the-shelf components available in the institute premises. The system operates at 2.5GHz transmit and 5GHz receive frequency. The maximum detectable range of the developed radar was 3.84m for a monostatic configuration. The bistatic radar configuration using broadband high gain horn antennas was identified for superior performance in detection of the tag over an area-under-test (the mosquito net) for laboratory experiments. Empirical tests determined a probability of detection of 88.25% and probability of false alarm of 0.29% for a signal threshold of -107.5dBm.

5.1 Current hardware limitations

The range of operation of the first generation harmonic radar can be improved by transmitting higher power and deploying higher gain transmitting and receiving antennas. Table 5.1 compares the radar parameters (transmitted power, transmitting and receiving antenna gain, detectable range) of the harmonic radar system deployed for field study in [1] and the system developed in this thesis. Also, to transmit high power (in kW range), licence clearance would be required.

TABLE 5.1: Comparison of radar parameters of system deployed for field study in [1] and the radar developed in this thesis

Radar parameters	**Radar deployed in [1]**	**Radar developed in thesis**
Transmitted power	25 kW	1 W
Transmitter antenna gain	30 dB	8.91 dBi
Receiver antenna gain	30 dB	10.02 dBi
Maximum detectable range	700 m	3.84 m

5.2 Future Work

The future work involves upgrading the system from narrowband to broadband in order to support range estimation of the insect target. Further, the single channel receiver system can be upgraded to a multiple channel system with a receiver antenna array to support direction-of-arrival estimation of the target. Naturally, the improved radar functionalities will trade off with increased hardware cost and complexity.

Bibliography

[1] J. Riley, A. Smith, D. Reynolds, A. Edwards, J. Osborne, I. Williams, N. Carreck, and G. Poppy, "Tracking bees with harmonic radar," *Nature*, vol. 379, no. 6560, p. 29, 1996.

[2] C. Eardley, D. Roth, J. Clarke, S. Buchmann, B. Gemmill *et al.*, *Pollinators and pollination: a resource book for policy and practice.* Agricultural Research Council (ARC), 2006.

[3] M. Aizen and P. Feinsinger, "Bees not to be? responses of insect pollinator faunas and flower pollination to habitat fragmentation," in *How landscapes change.* Springer, 2003, pp. 111–129.

[4] H. Abou-Shaara, "The foraging behaviour of honey bees, apis mellifera: a review." *Veterinarni medicina*, vol. 59, no. 1, 2014.

[5] J. L. Woodgate, J. C. Makinson, K. S. Lim, A. M. Reynolds, and L. Chittka, "Lifelong radar tracking of bumblebees," *PloS one*, vol. 11, no. 8, p. e0160333, 2016.

[6] S. Klein, C. Pasquaretta, X. J. He, C. Perry, E. Søvik, J.-M. Devaud, A. B. Barron, and M. Lihoreau, "Honey bees increase their foraging performance and frequency of pollen trips through experience," *Scientific reports*, vol. 9, no. 1, p. 6778, 2019.

[7] C. W. Schneider, J. Tautz, B. Grünewald, and S. Fuchs, "Rfid tracking of sublethal effects of two neonicotinoid insecticides on the foraging behavior of apis mellifera," *PloS one*, vol. 7, no. 1, p. e30023, 2012.

[8] A. Decourtye, J. Devillers, P. Aupinel, F. Brun, C. Bagnis, J. Fourrier, and M. Gauthier, "Honeybee tracking with microchips: a new methodology to measure the effects of pesticides," *Ecotoxicology*, vol. 20, no. 2, pp. 429–437, 2011.

[9] D. F. Minahan and J. Brunet, "Strong interspecific differences in foraging effort observed between honey bees and bumble bees using miniaturized radio frequency identification (rfid)." *Frontiers in Ecology and Evolution*, vol. 6, p. 156, 2018.

[10] P. Nunes-Silva, M. Hrncir, J. Guimarães, H. Arruda, L. Costa, G. Pessin, J. Siqueira, P. De Souza, and V. Imperatriz-Fonseca, "Applications of rfid technology on the study of bees," *Insectes sociaux*, vol. 66, no. 1, pp. 15–24, 2019.

[11] J. Riley and A. Smith, "Design considerations for an harmonic radar to investigate the flight of insects at low altitude," *Computers and Electronics in Agriculture*, vol. 35, no. 2-3, pp. 151–169, 2002.

[12] D. Milanesio, M. Saccani, R. Maggiora, D. Laurino, and M. Porporato, "Recent upgrades of the harmonic radar for the tracking of the asian yellow-legged hornet," *Ecology and evolution*, vol. 7, no. 13, pp. 4599–4606, 2017.

[13] S. Wolf, D. P. McMahon, K. S. Lim, C. D. Pull, S. J. Clark, R. J. Paxton, and J. L. Osborne, "So near and yet so far: harmonic radar reveals reduced homing ability of nosema infected honeybees," *Plos one*, vol. 9, no. 8, p. e103989, 2014.

[14] E. A. Capaldi, A. D. Smith, J. L. Osborne, S. E. Fahrbach, S. M. Farris, D. R. Reynolds, A. S. Edwards, A. Martin, G. E. Robinson, G. M. Poppy *et al.*, "Ontogeny of orientation flight in the honeybee revealed by harmonic radar," *Nature*, vol. 403, no. 6769, p. 537, 2000.

[15] D. W. Williams, G. Li, and R. Gao, "Tracking movements of individual anoplophora glabripennis (coleoptera: Cerambycidae) adults: application of harmonic radar," *Environmental entomology*, vol. 33, no. 3, pp. 644–649, 2004.

[16] J. C. Makinson, J. L. Woodgate, A. Reynolds, E. A. Capaldi, C. J. Perry, and L. Chittka, "Harmonic radar tracking reveals random dispersal pattern of bumblebee (bombus terrestris) queens after hibernation," *Scientific reports*, vol. 9, no. 1, p. 4651, 2019.

[17] N. Carreck, "The use of harmonic radar to track flying bees," *Bee Craft (United Kingdom)*, 1996.

[18] K. Rasilainen and V. V. Viikari, "Transponder designs for harmonic radar applications," *International Journal of Antennas and Propagation*, vol. 2015, 2015.

[19] R. Brazee, E. Miller, M. Reding, M. Klein, B. Nudd, and H. Zhu, "A transponder for harmonic radar tracking of the black vine weevil in behavioral research," *Transactions of the ASAE*, vol. 48, no. 2, pp. 831–838, 2005.

[20] I. S. Merrill *et al.*, "Introduction to radar systems," *Mc Grow-Hill*, vol. 7, no. 10, 2001.

[21] K. A. Gallagher, G. J. Mazzaro, A. F. Martone, K. D. Sherbondy, and R. M. Narayanan, "Derivation and validation of the nonlinear radar range equation," in *Radar Sensor Technology XX*, vol. 9829. International Society for Optics and Photonics, 2016, p. 98290P.

[22] Z. Ma, K. Nomiyama, and Y. Kobayashi, "Microstrip lowpass filters with reduced size and improved stopband characteristics," *IEICE transactions on electronics*, vol. 88, no. 1, pp. 62–67, 2005.

[23] G. M. Aji, M. A. Wibisono, and A. Munir, "High gain 2.4 ghz patch antenna array for rural area application," in *2016 22nd Asia-Pacific Conference on Communications (APCC)*. IEEE, 2016, pp. 319–322.

[24] K. Khandelwal and A. Kureshi, "Realization of microstrip band-pass filter design," *Int J Adv Res Comput Eng Technol (IJARCET)*, vol. 3, no. 12, pp. 4242–4247, 2014.

[25] O. Chaudhary and R. Chand, "Economic benefits of animal pollination to indian agriculture," *Indian Journal of Agricultural Sciences*, vol. 87, no. 9, pp. 1117–38, 2017.

[26] H. Human, R. Brodschneider, V. Dietemann, G. Dively, J. D. Ellis, E. Forsgren, I. Fries, F. Hatjina, F.-L. Hu, R. Jaffé *et al.*, "Miscellaneous standard methods for apis mellifera research," *Journal of Apicultural Research*, vol. 52, no. 4, pp. 1–53, 2013.